

See discussions, stats, and author profiles for this publication at: <https://www.researchgate.net/publication/311518719>

# Adaptation in Variable Parallel Compliance: Towards Energy Efficiency in Cyclic Tasks

Article in IEEE/ASME Transactions on Mechatronics · December 2016

DOI: 10.1109/TMECH.2016.2637826

CITATIONS

18

READS

447

4 authors, including:



**Rezvan Nasiri**

University of Waterloo

19 PUBLICATIONS 77 CITATIONS

[SEE PROFILE](#)



**Mahdi Khoramshahi**

École Polytechnique Fédérale de Lausanne

49 PUBLICATIONS 291 CITATIONS

[SEE PROFILE](#)



**Mohammad Shushtari**

University of Tehran

5 PUBLICATIONS 29 CITATIONS

[SEE PROFILE](#)

Some of the authors of this publication are also working on these related projects:



Exoskeletons, a new future!! [View project](#)



Energy Efficiency in Bio-inspired Locomotion with Cyclic Nature [View project](#)

# Adaptation in Variable Parallel Compliance: Towards Energy Efficiency in Cyclic Tasks

Rezvan Nasiri, Mahdi Khoramshahi\*, Mohammad Shushtari, and Majid Nili Ahmadabadi\*\*

**Abstract**—We present a compliance adaptation method for online natural dynamics modification of multi-joint robots performing cyclic tasks. In this method, parameters of multi-basis nonlinear compliances, acting in parallel with actuators, are adapted to minimize actuation forces which results in joint-by-joint energy consumption reduction. Stability, convergence, and optimality of this method are proved analytically for a general compliance structure. We do not impose any specific constraint on the controller structure and tracking performance, yet stable tracking of cyclic motions is necessary for the convergence to the optimal solution. Extensive simulations on a set of systems, ranging from simple mass-spring system to robotic manipulator (with linear and nonlinear compliances), along with the experimental results on a 1-DOF compliant revolute joint with two basis functions in the compliance profile, demonstrate the efficiency of our method in terms of stability, convergence, and optimality; i.e., actuation force and energy consumption reduction.

**Index Terms**—Adaptive compliance, nonlinear compliance, natural dynamics, energy efficiency, cyclic tasks

## I. INTRODUCTION

WE are witnessing numerous and remarkable achievements in developing sophisticated actuation mechanisms for robotic applications. With the aim of safety, stability, and energy efficiency, many designers incorporate compliant elements in their mechanisms, in parallel or in serial configurations [1-4]. Moreover, thanks to the recent advancements in Variable stiffness Actuators (VSAs) [5-7], there is no major limitation to employ nonlinear compliances which can be tuned online [7-9]. In other words, we can benefit from nonlinear Variable Stiffness Actuators (VSAs). Nevertheless, despite these achievements in design and fabrication of compliant systems/robots, there is still no general and systematic method to adapt nonlinear compliant elements to attain energy efficiency. This work addresses this issue by proposing a stable and optimal adaptation method for parallel variable compliances in cyclic tasks.

At a robotic joint, compliance can appear in two configurations: serial and parallel. Both configurations can be advantageous; see [10] and [11] for comparisons. Nevertheless, higher order dynamics in serial configuration encumbers the control and the mathematical analysis. On the other hand, additive relation between actuator and compliance forces in the parallel configuration results in a simpler mechanism and mathematics; see [12]. This property enables us to propose a

simple, but powerful energy-efficiency-seeking adaptation rule for parallel compliances.

Studies in energetic cost of locomotion, showed us that compliant elements have a tremendous impact on the natural dynamics and energy consumption; see [13]. In the 90s, the importance of compliant elements in the locomotion of some legged animals was pinpointed [14] which, in a few years, set motion to the new field of compliant robotics where many robots with compliant legs and spines have been implemented; see [15-18]. Moreover, there are numerous studies suggesting that animals (and human) actively adapt their body stiffness –including legs– to their task and environment especially for energy efficiency; see [19] and [20]. Inspired by nature, our proposed method adapts the parallel compliance to a given cyclic task to reach lower energy consumption; i.e., shaping/modifying the natural dynamics according to the task.

Since the introduction of passive walkers to the robotics community, see [21] as the pioneering work, utilizing passive/natural dynamics for energy efficiency has been the main goal of many researchers [22]. Nonetheless, systematic exploitation of natural dynamics in complex systems is not straightforward. Natural dynamics exploitation can be executed in the level of controller [23] or in the level of motion generation [24]. In our previous works, [24] and [25], we introduced the Linear and Nonlinear Adaptive Natural Oscillators (ANO and NANO) to tune the frequency and the shape of cyclic motions for energy efficiency. Nonetheless, for a given task and a fixed natural dynamics, exploitative trajectories are highly limited. Therefore, beside trajectory adaptation, natural dynamics modification/adaptation is necessary to attain a lower energy consumption. In natural dynamic modification/adaptation, we adapt the dynamics according to the desired trajectory. In this work, we particularly focus on the adaptation of joints compliance for energy consumption reduction.

The related works are reviewed in the next section. We formulate the problem and propose the adaptation rule in Section III. Mathematical analyses are presented in Section IV where we study the convergence behavior and the energy minimization properties of our method. In Section V, the performance of the proposed method is studied in comprehensive simulations, ranging from simple to complex robotic systems. Experimental results of a 1-DOF revolute joint with parallel variable compliance are presented in Section VI. Discussions and conclusions are presented in the last two sections.

## II. RELATED WORK

In robotics, especially in legged systems, several heuristic methods are presented for *offline* compliance design; see

\*Corresponding author; e-mail: m80.khoramshahi@gmail.com

\*\*Principal corresponding author; e-mail: mnili@ut.ac.ir

All authors are with Cognitive Systems Laboratory, Control and Intelligent Processing Center of Excellence (CIPCE), School of Electrical and Computer Engineering, College of Engineering, University of Tehran, Iran.

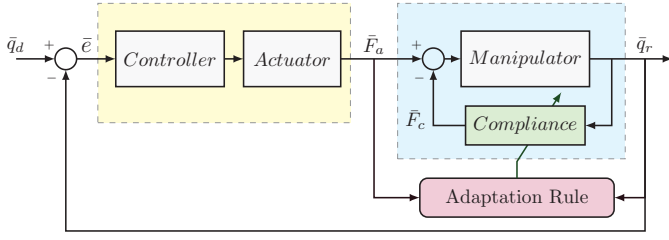


Fig. 1. Control schematic for an  $n$ -DOF robotic manipulator with parallel adaptive compliance at joints. All variables are  $n \times 1$  vectors.

[26-29]. In this fashion, besides compliance, task-relevant trajectories can also be optimized; see [4], [30], and [31]. Another strategy is to optimize compliance and mass distribution simultaneously; see [32]. In a previous work [33], we proposed an *offline* method to design parallel compliance so as to improve energy efficiency in cyclic motions. In this paper, we tackle the same problem in an *online* regime.

Variable compliance actuators are utilized in bipedal robots to reduce the energy consumptions; see [34] and [35]. Moreover, a tuning method is also presented in [34, chap. 5]; where compliance is tuned based on the partial derivative of force with respect to trajectory. This method is now widely used in robotic applications; see [34-36]. Nevertheless, using force derivatives is not only prone to noise, but also causes large unsettling oscillations in the compliance structure and dissipates energy. Moreover, lack of equilibrium and endless variation of stiffness has shown to be inefficient [34, pp. 199]. However, using same quantities as in [34], applied forces and input trajectories, we present a stable and efficient compliance adaptation method.

An *online* adaptation method for linear elasticity in 1-DOF revolute joint has been introduced in [37]. Recently, this method has been adopted to multi-joint manipulators and extended to motion learning regimes; see [12] and [38]. These methods are shown to be stable and optimal only when the structure of the controller is presupposed. Moreover, they are limited to linear compliance structures. In contrast, we consider our adaptation method as general for three main reasons: (1) we do not impose any constraint on the controller as long as tracking performance is satisfactory, (2) our method is independent from the compliance structure; i.e., it handles both linear and nonlinear cases, and (3) by means of multi-basis nonlinear compliance, we have more degrees of freedom in order to decrease energy consumption. To highlight these aspects, we place our method under more analytical scrutiny in terms of stability, convergence, and optimality in the following sections. In addition, we present comparative simulations and experimental results (in Section V and Section VI) so as to clarify superiority of nonlinear adaptive compliance (our method) over linear ones.

### III. PROBLEM STATEMENT AND ADAPTATION RULE

Consider Fig. 1 as a general control system for an  $n$ -DOF robotic manipulator. In this system,  $\bar{q}_r \in \mathbb{R}^n$  is the joint position and the desired  $T$ -periodic<sup>1</sup> and smooth trajectory

<sup>1</sup> $T$  is the period of cyclic motion and  $x(t)$  is periodic if  $x(t \pm T) = x(t)$ .

( $\bar{q}_d \in \mathbb{R}^n$ ) is given<sup>2</sup>. The controller tries to minimize tracking error ( $\bar{e} \in \mathbb{R}^n$ ) using applied force ( $\bar{F}_a \in \mathbb{R}^n$ ). Parallel to each joint ( $j = 1, \dots, n$ ), there is a variable/adaptable compliance ( $\bar{K}_j(\cdot)$ ) that exerts force  $F_{c_j}$  ( $\bar{F}_c \in \mathbb{R}^n$ ). The problem is to find an adaptation rule for compliant elements to improve energy efficiency.

**Definition 1** (Compliance force representation). *Compliance force in the  $j$ th joint is defined in the following general form*

$$F_{c_j}(t) = \bar{K}_j^T \bar{\Phi}_j = \sum_{i=1}^m k_{ij} \phi_{ij}(q_{r_j}(t)) \quad ; \quad \bar{K}_j, \bar{\Phi}_j \in \mathbb{R}^m \quad (1)$$

where, for  $j$ th joint,  $k_{ij}$  is the coefficient and  $\phi_{ij}$  is the corresponding passive and sufficiently smooth basis function defined over the joint position.

By choosing a proper set of basis functions (e.g., polynomials), Eq. 1 acts as a general function approximator; see [39, pp. 923]. Note that the basis functions ( $\bar{\Phi}_j$ ), which define the compliance structure, are fixed and compliance coefficients<sup>3</sup> ( $\bar{K}_j$ ) are adaptable. In this representation, the compliance force is linear w.r.t. the adaptable coefficients while it can be nonlinear w.r.t. the joint position due the selection of the basis functions. This allows for simple adaptive laws for nonlinear compliant elements. By choosing  $\bar{\Phi}_j = [q_{r_j}]$ , we have a linear spring, and by  $\bar{\Phi}_j = [q_{r_j} \ q_{r_j}^2 \ \dots \ q_{r_j}^m]^T$ , we represent a polynomial compliance. Pre-compression can be included by having a unit basis function ( $\phi_{ij} = 1$ ).

**Definition 2** (Adaptation rule). *Adaptation rule for compliance coefficients at the  $j$ th joint is proposed as*

$$\dot{\bar{K}}_j = -\epsilon F_{a_j} \bar{\Phi}_j \quad (2)$$

where  $\epsilon$  is the adaptation rate, and  $F_{a_j}$  is the applied force at the  $j$ th joint.

The proposed method only utilizes the applied forces and joint positions, and does not require any knowledge of the control system or dynamical equations of the robot. Moreover, the adaptation takes place locally at the joint level.

### IV. MATHEMATICAL ANALYSIS

Consider the dynamical equations of a  $n$ -DOF manipulator system with parallel compliance at each joint.

$$H(\ddot{q}_r, \dot{q}_r, \bar{q}_r) = \bar{F}_a(t) - \bar{F}_c(t) \quad ; \quad H : \mathbb{R}^{n \times n \times n} \rightarrow \mathbb{R}^n \quad (3)$$

The desired force ( $F_d$ ), which is necessary to track the desired trajectory ( $q_d$ ), can be calculated as follows.

$$\bar{F}_d = H(\ddot{q}_d, \dot{q}_d, \bar{q}_d) \quad (4)$$

Using Eq. 3 and Eq. 4, the applied force can expressed as

$$\bar{F}_a = \bar{F}_d + \bar{F}_c + \bar{F}_e \quad ; \quad \bar{F}_e = H(\ddot{q}_r, \dot{q}_r, \bar{q}_r) - H(\ddot{q}_d, \dot{q}_d, \bar{q}_d) \quad (5)$$

where error-force ( $\bar{F}_e$ ) is added due to imperfection of the controller/actuator. In case of perfect tracking ( $\bar{q}_r \equiv \bar{q}_d$ ), we have  $\bar{F}_e \equiv 0$ .

<sup>2</sup>In our notation,  $\bar{x}$  is a vector whereas  $x$  is just a scalar.

<sup>3</sup> $K$  is in fact the vector of compliant element's coefficients. Nevertheless, for the sake of simplicity, we refer to it as compliance coefficients.

**Assumption 1** (Bounded error). *The controller can satisfy bounded tracking error and bounded error-force ( $\|\bar{e}\|_\infty < \gamma_e$  and  $\|\bar{F}_e\|_\infty < \gamma_f$ ). Bounded error ( $\bar{e}$ ) and desired trajectory ( $\bar{q}_d$ ) result in bounded joint position ( $\|\bar{q}_r\|_\infty < \gamma_r$ ). Where  $\gamma_e$ ,  $\gamma_f$ , and  $\gamma_r$  are upper bounds for tracking error, error-force, and joint position respectively.*

For the sake of simplicity, and without loss of generality, we focus on one coordinate to study the convergence behavior of adaptation. For any of the coordinates,  $q, q_d \in \mathbb{R}$  are the real and the desired joint positions respectively.  $e, \dot{e} \in \mathbb{R}$  are tracking error and its time derivative.  $K \in \mathbb{R}^m$  is the vector of compliance coefficients.  $\Phi, \Phi_d \in \mathbb{R}^m$  are the vectors of compliance basis functions as a function of the real and the desired joint positions respectively.  $F_a, F_d, F_c, F_e \in \mathbb{R}$  are the applied, desired, compliance, and error-force respectively.

**Theorem 1** (Desired force decomposition). *The desired force can be decomposed as*

$$F_d = -\tilde{K}^T \Phi_d + F_{res} ; \quad \tilde{K} \in \mathbb{R}^m, F_{res} \in \mathbb{R} \quad (6)$$

where the projection coefficients ( $\tilde{K}$ ) are calculated by projecting the desired force onto basis functions as

$$\tilde{K} = -\Omega \int_T F_d \Phi_d dt ; \quad \Omega = \left( \int_T \Phi_d \Phi_d^T dt \right)^{-1} \in \mathbb{R}^{m \times m} \quad (7)$$

where  $\Omega$  exists if and only if the basis functions ( $\Phi_d$ ) are linearly independent (see [Appendix-A](#)). It can be shown that this decomposition minimizes  $F_{res}$  over a cycle and has the following property.

$$\int_T F_{res} \Phi_d dt = 0 \quad (8)$$

*Proof.* see [Appendix-B](#).  $\square$

The residual force ( $F_{res}$ ) is the part of the desired force which cannot be generated by the compliance ( $\tilde{K}$  and  $\Phi_d$ ). Interestingly, [Eq. 7](#) can be used for computing the optimum coefficients of the basis functions in an offline manner which requires dynamics of the system; see [Appendix-C](#). However, in the online adaptation, only the instantaneous applied force ( $F_a$ ) and joint position ( $q$ ) are required.

**Proposition 1** (Adaptation dynamics). *Using the presented decomposition, the adaptation rule ([Eq. 2](#)) can be expressed as*

$$\dot{K} = -\epsilon (\Phi \Phi^T K - \Phi \Phi_d^T \tilde{K} + \Phi (F_{res} + F_e)) \quad (9)$$

*For derivation.* see [Appendix-D](#).  $\square$

**Theorem 2** (Stability and convergence). *The dynamical system described in [Eq. 9](#)*

- 1) *is stable*
- 2) *for periodic motions,  $K$  converges on average<sup>4</sup>.*
- 3) *in perfect tracking,  $K$  converges to  $\tilde{K}$  on average.*

*Proof.* see [Appendix-E](#).  $\square$

The troublesome term  $F_{res}$  in [Eq. 9](#) has a direct impact on the magnitude of oscillations around the average solution. To

have smaller  $F_{res}$ , proper selection/design of basis functions (proper compliance profile) is needed. In the case of perfect tracking ( $F_e \equiv 0$ ),  $F_{res} \equiv 0$  is an interesting special case where the average and the exact solutions are equal; i.e.,  $K$  converges exactly to  $\tilde{K}$ . Therefore, by comparing [Eq. 6](#) and [Eq. 5](#), it can be concluded that after convergence,  $F_a$  diminishes to zero meaning that the desired force is fully generated by the compliant element; i.e., the task is performed without any active effort ( $F_a \equiv 0$ ). For a given set of basis functions ( $\Phi$ ), we call a desired motion ( $q_d$ ) resulting in  $F_{res} \equiv 0$  *Compliance Consistent Motion* (CCM). We name the other ones *Compliance Inconsistent Motion* (CIM). The inconsistency between the motion (i.e., the task) and the compliance (i.e., the natural dynamics) can be measured by the steady-state residual force. This measure also can be utilized to improve the design of the compliant mechanism (i.e., the basis functions) to further energy consumption reduction.

**Theorem 3** (Optimality). *The adaptation rule ([Eq. 2](#)):*

- 1) *minimizes the following cost function:*

$$J(t) = F_a^2(t) \quad (10)$$

*which means that compliance adaptation is equivalent to instantaneous applied force minimization.*

- 2) *for periodic motions, on average, minimizes the following cost function:*

$$J_T(t) = \int_{t-T}^t F_a^2(u) du \quad (11)$$

*Proof.* see [Appendix-F](#).  $\square$

**Corollary 1** (PD-Controller). *In case of the PD controller (with  $k_p$  and  $k_d$  as proportional and derivative gains), the adaptation rule ([Eq. 2](#))*

- 1) *results in  $(k_p e + k_d \dot{e})^2$  minimization.*
- 2) *for periodic motions, on average, minimizes the following cost function.*

$$\int_{t-T}^t (k_p^2 e^2(u) + k_d^2 \dot{e}^2(u)) du \quad (12)$$

*Proof.* see [Appendix-G](#).  $\square$

According to [Corollary 1](#), tracking performance improves along with adaptation which provides better condition for adaptation itself. This *tracking-adaptation* cooperative behavior leads to a better closed loop performance. In the next section, we see how compliance adaptation for CCM cases, even in presence of a non-perfect controller (PID controller), leads to perfect tracking and exact convergence ( $F_a \equiv F_{res} \equiv 0$ ). In CIM cases, however, it leads to  $F_a \equiv F_{res} + F_e$  on average.

**Corollary 2** (Mechanical energy consumption minimization). *Under the perfect-tracking assumption, the proposed adaptation rule ([Eq. 2](#)) attempts to reduce the instantaneous mechanical energy consumption ( $|F_a \dot{q}|$ ). *Proof.* see [Appendix-H](#).  $\square$*

It can be inferred from [Eq. 9](#) that lowering  $\epsilon$  reduces the magnitude of oscillations induced by  $F_{res}$  and  $F_e$ . On the other hand, [Eq. 9](#) also implies that the speed of convergence is proportional to  $\epsilon$ . This *ripple-speed* trade-off can be settled by the design and control criteria. However, for further improvements, a decaying adaptation rate can be imagined which lays

<sup>4</sup>Average of  $x(t)$  is defined as  $x_{avg}(t) = \frac{1}{T} \int_{t-T}^t x(s) ds$ .

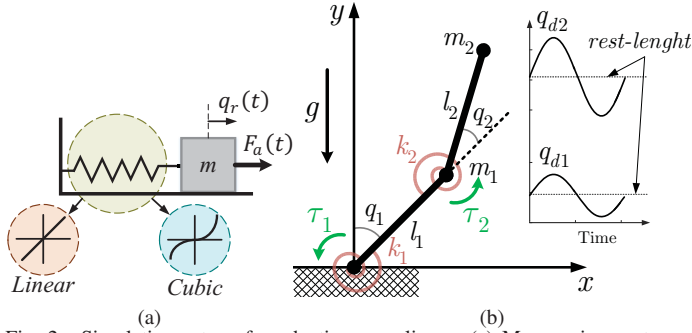


Fig. 2. Simulation setups for adaptive compliance. (a) Mass-spring system where the spring can have different profiles; linear or cubic. In all cases, mass ( $m$ ) is  $1kg$ , and  $F_a(t)$  is the force applied by a PID controller with the following gains:  $k_p = 100$ ,  $k_i = 1$ , and  $k_d = 10$ . (b) A 2-DOF manipulator with parallel adaptive compliances at its joints. In this simulation we consider two different compliance profiles; linear and piecewise linear. The rest-length of the compliances in the first and the second joints are set to  $\pi/6rad$  and  $2\pi/3rad$  respectively; i.e., in the middle of the desired trajectory. Here, we have  $m_1 = m_2 = 1kg$ ,  $l_1 = l_2 = 1m$ , and  $g = 9.81m/s^2$ .  $\tau_1$  and  $\tau_2$  are torques applied by the PID controllers ( $k_p = 100$ ,  $k_i = 10$ , and  $k_d = 50$ ).

outside the scope of this paper. Besides, based on Eq. 9, the convergence behavior (i.e., settling time) depends on the joint trajectories and the basis functions; i.e.,  $\Phi\Phi^T$  and especially the off-diagonal values of this matrix. Therefore, adaptation rate ( $\epsilon$ ) needs to be re-tuned case by case. To have a similar convergence behavior for a given  $\epsilon$  across different cases, we propose the following normalized adaptation rule.

**Definition 3** (Normalized adaptation rule). *Normalized adaptation rule for compliance coefficients is*

$$\dot{K} = -\epsilon\Omega\Phi F_a \quad (13)$$

**Theorem 4.** *The normalized adaptation rule results in uncoupled and normalized dynamics with stable and optimal convergence. Proof. see Appendix-I.  $\square$*

The normalized adaptation rule is applicable when the trajectory is known; it is the case in cyclic and non-time-varying tasks. Otherwise  $\Omega$  in Eq. 7 cannot be calculated. The normalized rule is advantageous over the original one (Eq. 2) when  $\Omega \neq cI$ , where  $c$  is a scalar and  $I$  is the identity matrix.

## V. SIMULATIONS

In this section, we investigate the performance of the proposed adaptation method in a set of simulations; see Fig. 2. In order to achieve the similar convergence time, in all simulations, the normalized adaptation rule (Eq. 13) is utilized with  $\epsilon = 1$ . The simulations are performed using Matlab/Simulink/Simmechanis [40].

### A. Mass-spring

In this section, as an insightful example, we start with mass-spring systems with different types of compliances (Fig. 2a). The difference between the setups is in the compliance force-displacement profiles; i.e., basis functions ( $\Phi$ ). We consider two different types of compliances: linear and nonlinear. The desired trajectory ( $q_d$ ) for this simulation is generated by a motion generator with dynamical equation as  $\ddot{q}_d = -\tilde{K}^T \Phi_d$ .

Initial conditions for the motion generator and the mass-spring systems are  $q_d = 1m$  and  $\dot{q}_d = 0m/s$ . The reference trajectory is generated by the motion generator when  $\Phi_d = [q_d \ q_d^3]^T$  and  $\tilde{K} = [2 \ 1]^T$ . For comparison, we consider three different cases: the non-compliant, the linear compliance ( $\Phi = [q]$ ), and the nonlinear compliance ( $\Phi = [q \ q^3]$ ). Clearly, the reference trajectory is CCM for the nonlinear case, while it is CIM for the linear one. The results are illustrated in Fig. 3. According to Fig. 3a, in the nonlinear case, the coefficients exactly converge to their optimum values ( $K = [2 \ 1]^T$  as in the motion generator), while in the linear case, the coefficient converges with small fluctuations. These fluctuations attest that for the linear spring, the reference trajectory is CIM. Moreover, the average converged value can be explained by decomposition of the desired force (Eq. 6) as

$$F_d = -2q_d - q_d^3 = -2.74q_d - \underbrace{(q_d^3 - 0.74q_d)}_{F_{res}}; \quad \int_T q_d F_{res} dt = 0$$

This equation along with Fig. 3a confirm that the linear compliance, on average, converges to its theoretical value as discussed in Section IV. Also, by adapting linear compliance, the controller effort is reduced significantly compared to the non-compliant case; i.e., it converges to residual force ( $F_{res}$ ). Whereas in the nonlinear case, the controller force diminishes to zero due to consistency between the reference trajectory and the compliance; see Fig. 3b. Fig. 3c shows a comparison between the total energy consumption<sup>5</sup>; see Appendix-J for computational details. Accordingly, adaptation in the linear(nonlinear) reduces the energy consumption by 75%(100%). Finally, Fig. 3d shows that the tracking error reduces drastically for the linear case, and vanishes to zero for the nonlinear one.

### B. Manipulator

In this section, we investigate the behavior of our adaptation method for simultaneous adaptation of several parallel compliances in a more complicated system; i.e., a 2-DOF manipulator with the adaptive compliances at its joints as shown in Fig. 2b. To draw a comparison between linear and nonlinear compliant structures in terms of energy efficiency, we consider three different cases: non-compliant, the linear compliance ( $\Phi = [q]$ ), and the piecewise linear compliance ( $\Phi = [qu(q) \ qu(-q)]^T$ )<sup>6</sup>.

The task is to move the end-effector on an oval centered at  $O = (0m, 1m)$  with radius  $r_x = 0.2m$ ,  $r_y = 0.5m$  and frequency  $\omega = 6rad/s$ . The reference trajectory is tracked by solving the inverse kinematics in elbow-down position and a PID controller. In all cases, position of the end-effector is initialized on the reference trajectory and the initial values for compliance coefficients are zero.

The simulation results for the manipulator system are reported in Tab. I. While convergent behaviors are achieved, the ripples are smaller in the nonlinear cases compared to the linear one. Moreover, these results show that the nonlinear compliance leads to a lower applied forces as well as

<sup>5</sup>Total energy = required energy for adaptation + mechanical energy.

<sup>6</sup> $u(\cdot)$  is the step function.

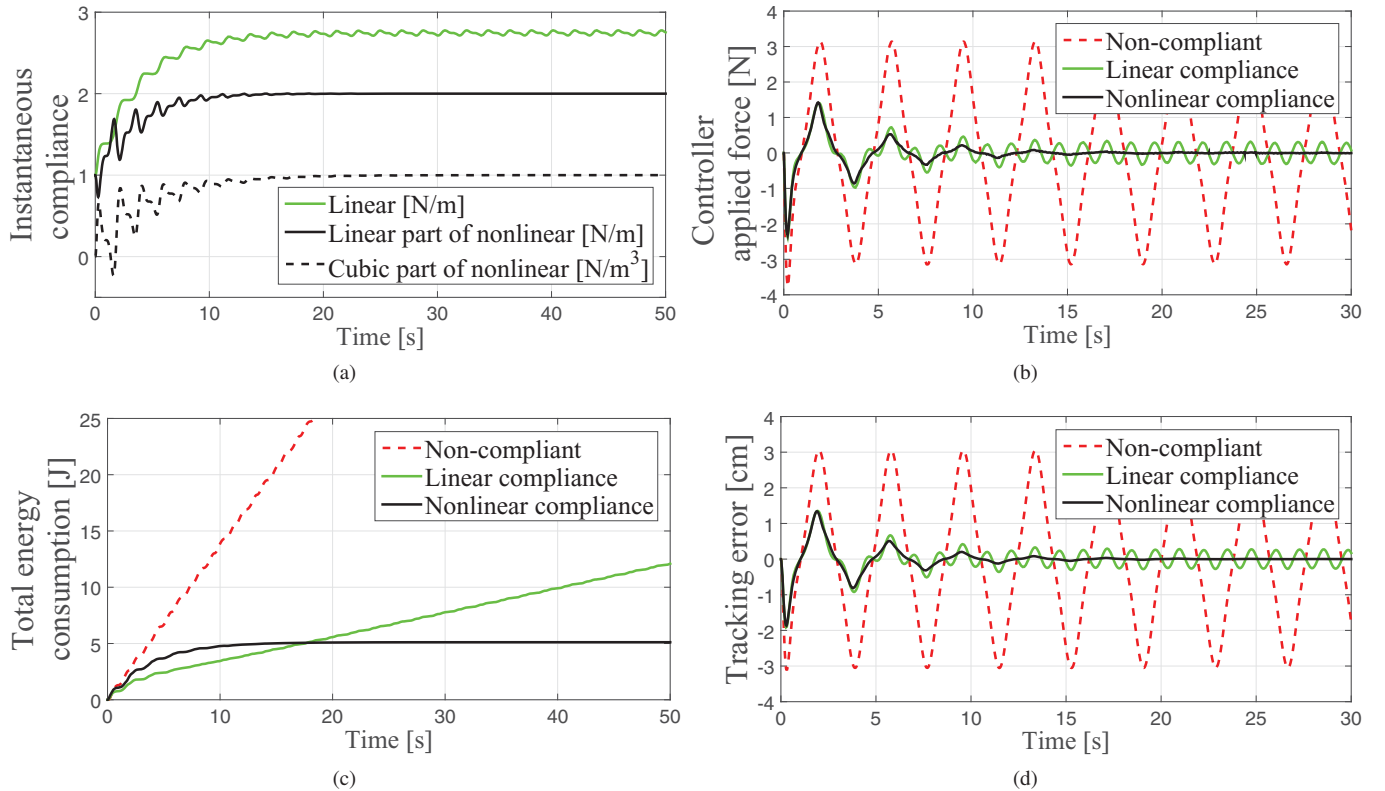


Fig. 3. Comparison between linear and cubic basis functions for the mass-spring system for a motion profile generated using a nonlinear spring.

TABLE I

LINEAR AND NONLINEAR COMPLIANCE ADAPTATION IN THE 2-DOF MANIPULATOR. THE RESULTS ARE PRESENTED IN THE STEADY-STATE CONDITION REACHED APPROXIMATELY IN 5s.

|                           | Joint  | Representation      | Dimension          | Non-compliant | Linear compliance | Nonlinear compliance          |
|---------------------------|--------|---------------------|--------------------|---------------|-------------------|-------------------------------|
| Compliance coefficient(s) | First  | Mid $\pm$ Deviation | [Nm/rad]           | —             | $57 \pm 9$        | $(12 \pm 3), (97 \pm 3)$      |
|                           | Second | Mid $\pm$ Deviation | [Nm/rad]           | —             | $26 \pm 6$        | $(51.5 \pm 1.5), (8 \pm 1.5)$ |
| Applied torque            | First  | RMS                 | [Nm]               | 18.1          | 11.7              | 5.7                           |
|                           | Second | RMS                 | [Nm]               | 15.9          | 10.3              | 4.3                           |
| Tracking error            | First  | RMS                 | [rad] $\times$ 100 | 4.8           | 2.4               | 1.6                           |
|                           | Second | RMS                 | [rad] $\times$ 100 | 4.1           | 1.6               | 1.1                           |
| Power consumption         | Total  | Mean                | [J/s]              | 46.4          | 35.2              | 19.2                          |

tracking errors; i.e., a higher consistency between the motion and the compliance. Finally, using the non-compliant case as the baseline, the nonlinear case results in 58% energy consumption reduction whereas the linear one results only in 25% improvement.

## VI. EXPERIMENTAL RESULTS

1) *Setup*: To investigate the adaptation method in practice, we employ a 1-DOF revolute joint with variable compliance which has two basis functions; see Fig. 4. The revolute joint is actuated by a DC-motor (with 12V terminal voltage and 0.5Nm maximum torque). The motor is non-back-drivable and its no-load current is about 100mA and its full-load current in maximum performance is about 600mA. The joint is controlled using PWM method. To create an adaptive nonlinear compliance structure, we use a pair of linear springs where their strain-lengths can be controlled independently using two worm-gear motors; see [8] for similar designs. The

maximum current of the worm-gear motors is 150mA at 12V. Aforementioned properties of the motors along with frictions and other uncertainties suggest a considerable deviation from the ideal cases.

To apply the adaptation method, it is necessary to identify the compliance structure; i.e., the basis functions that maps  $q$  to  $F_c$ . In this arrangement, for  $|q| < 30\text{Deg}$ , the force-displacement profiles can be numerically approximated<sup>7</sup> by  $F_c = K_1 \sin(3q)u(q) + K_2 \sin(3q)u(-q)$ <sup>8</sup>. In this equation  $K_1$  and  $K_2$  can be independently controlled by  $S_1$  and  $S_2$  such that change in the strain-lengths ( $S_1$  and  $S_2$ ) leads to change in compliance profile at the revolute joint. Interestingly, equal strain-lengths ( $K = K_1 = K_2$ ) results in an approximately linear spring (for  $|q| < 30\text{Deg}$ ) which can be adapted by the linear adaptation rule as  $\dot{K} = -\epsilon F_a q$  while adjusting  $S_1$  and

<sup>7</sup>Estimation is done by mean-squared-error of 0.014 and 4% relative error.

<sup>8</sup>Note that in this formulation,  $K_1$  and  $K_2$  are not actually spring constants, but two coefficients in units of Nm.

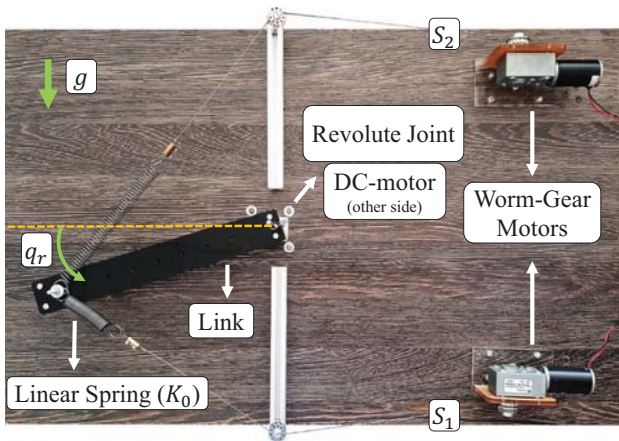


Fig. 4. The experimental setup with two adjustable linear springs. The strain lengths are controlled independently by the worm-gear motors. This arrangement of the linear springs allows for a variable nonlinear compliance at the revolute joint. The main actuator is mounted on the other side of the board and cannot be seen in this view.  $K_0$ ,  $S_1$ , and  $S_2$  are the stiffness and the strain-lengths of the linear springs. Finally,  $g$  and  $q_r$  denote the gravity and position vectors.

$S_2$  independently results in a nonlinear case; i.e., a piecewise linear compliance. This allows for a comparison between linear and nonlinear cases in terms of energy consumption. In this case, we have  $\Omega = cI$  and the adaptation rule (based on Eq. 2 or Eq. 13) is  $\dot{K}_1 = -\epsilon_1 q F_a u(q)$ ,  $\dot{K}_2 = -\epsilon_2 q F_a u(-q)$ .

In this experiment, the adaptation rates for the linear and the piecewise linear cases are set to  $\epsilon = 1$  and  $(\epsilon_1, \epsilon_2) = (1, 3)$  respectively, and the revolute joint position ( $q$ ) is provided by an encoder. We use the controller command instead of the applied force; see Section VII-D for discussions. We consider a sinusoidal oscillation ( $\omega = 9 \text{ rad/s}$  and  $A = 30 \text{ Deg}$ ) as the reference trajectory. The revolute joint moves in the vertical plane where the gravity makes this case CIM; i.e., the applied torque by the gravity cannot be fully compensated by the compliance during this task. The joint is controlled by a PID controller with  $k_p = 0.8$ ,  $k_i = 0.2$ , and  $k_d = 0.01$ .

2) *Results:* In this experiment, the compliance adaptation reduces the RMS tracking error from 2.6 [Deg] to 2.1 [Deg] for the linear, 2.15 [Deg] for the nonlinear case which supports Corollary 1 in practice. The Convergence behavior of both cases are plotted in Fig. 5a. Interestingly, in the piecewise linear case, the compliance in the negative(positive) displacements adapts to a low(high) stiffness. This shows that the effect of gravity on the natural dynamics can be exploited better by the nonlinear compliance.

To study the energy consumption of the actuator in the course of adaptation, we use the average input power. Having a switching terminal voltage (between 0 and 12) in the PWM method, this measure is proportional to the input current. Interestingly, in DC-motors, the applied torque is also proportional to the input current. Therefore, the applied-torque-minimization property of our method reflects a minimization behavior in the average input power. This fact can be seen in Fig. 5b where the piecewise linear compliance adaptation leads to a drastic decline in power consumption (about 35% improvement in comparison with the non-complaint case).

However, due to the high inconsistency between the reference path and the natural dynamics of the setup in the vertical plane, the linear compliance adaptation results only in 11% improvement compared to the non-compliant case. In addition, based on Fig. 5b, the compliance adaptation cost is larger for the linear case which is the result of higher ripples in the linear case which is the result of higher inconsistency between the desired trajectory and the basis function.

These experimental results show that our adaptation method is not only efficient, but also robust to the real-world uncertainties. In our setup, we do not use torque sensors due to their cost and noisy performance and we use simple controller and actuators. Despite all significant deviations form the ideal condition, our method not only works in practice, but also supports our aforementioned theories presented in Section IV.

## VII. DISCUSSIONS

We start this section by a comparison between adaptations in linear and nonlinear compliances. We also discuss the assumptions and limitations associated with our method in theory and practice, and we propose potential solutions.

### A. Comparison between linear and nonlinear compliances

In a typical robotic setup, due to nonlinearities in the dynamics or in the task, the desired torques are in a nonlinear relationship with the joint angles. Therefore, compliant mechanisms with nonlinear profiles have more flexibility to compensate these torques and consequently reduce the energy consumption. The presented evidences in this paper, both in simulation and practice, strongly support this fact. The improvement achieved in energy consumption by using a nonlinear compliance instead of a linear one is 100% for the simple setup in Section V-A, 33% for the simulated manipulator in Section V-B, and 24% for the experimental setup in Section VI. These improvements, along with the simplicity of our adaptation rule justify the use of nonlinear compliant mechanism; see also [41] for another comparison between linear and nonlinear compliances.

Recent innovative designs on the nonlinear compliances made it easy to construct nonlinear and adaptable compliances; see [5-9] and [42]. For instance, as shown in our experimental setup in Section VI, a simple combination of linear springs leads to a nonlinear compliance at the joint. By proposing a general adaptation mechanism, we address a demand imposed by the growing technology of VSAs; i.e., adaptive and optimal methods to exploit nonlinear compliant designs. To the best of our knowledge, before this study, adaptation methods for variable compliant structures were limited to linear cases; see [12] for a linear adaptation method.

### B. Damping effect and ripple rejection

Velocity-dependent part of the desired force ( $F_d$ ) cannot be compensated by compliant elements, and therefore, rests in the residual force ( $F_{res}$ ). Here, we specifically focus on a simple mass-spring-damper system with a sinusoidal desired trajectory ( $q_d = A \sin(\omega t)$ ). Based on Section IV,

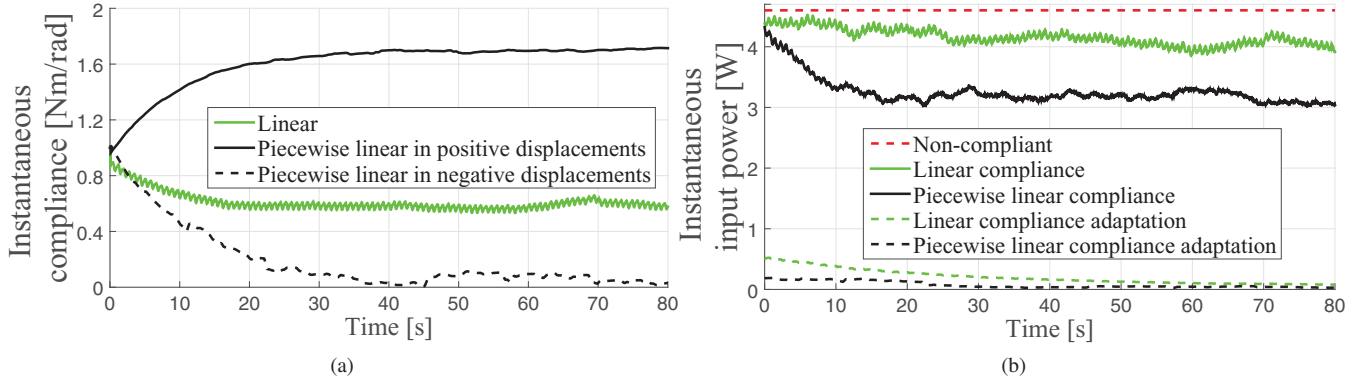


Fig. 5. Overall performance of compliance adaptation. (a) The variable compliance adaptation shows a convergent behavior. (b) Average input power is reduced during the adaptation for both cases. Interestingly, utilizing the piecewise linear compliance leads to a drastic improvement in comparison with the linear one. The first three items are the power consumed by the main actuator and the last two ones are for the compliance adaptation motors. It is important to note that figures are smoothed using a moving average window of 10s seconds (sampling rate is 100Hz).

the residual force is  $F_{res} = Ab\omega \cos(\omega t)$  where  $b$  is the damping coefficient, and the average power consumption is  $P_{avg} = b\omega^2 A^2/2$ . According to these equations the magnitude of ripples during the compliance adaptation and the magnitude of the residual force are proportional to the damping constant. Such ripples around the optimal value might be detrimental for the energy consumption for longer time horizons. One way to overcome the effect of residual force is to subtract it from the adaptation rule as  $\dot{K} = -\epsilon(F_a - F_{res}) \Phi$ . This modification leads to exact convergence (i.e., without ripples), but calculating the exact residual force is unrealistic. However, having a satisfactory estimation of damping in robotic joints is possible and beneficial to the compliance adaptation. Another possible solutions/compromises are to filter out the ripples or stop the adaptation, which lead to near-optimal solutions.

### C. Damped and constrained adaptation

Linear independency of the basis functions (i.e., inversion of  $\Omega$ ) is necessary condition for convergence. For singular and near-singular cases (i.e., improper choice/design of basis functions), we propose a damped adaptation rule method as  $\dot{K} = -\epsilon\Phi F_a - \beta K$ . Convergence proof and details of this method are presented in [Appendix-K](#). Moreover, in practice, the compliance coefficients are bounded ( $K_{min} < K < K_{max}$ ) rendering the adaptation into a constrained convex optimization. In other words, the convergence point is either the optimal solution of unconstrained problem, or on the boundaries.

### D. Force sensor and actuator saturation

One important component in the proposed method is the force signal which might requires a force sensor. In practice, precise force sensors are expensive. This issue can be considered as a limitation to our method. However, this problem can be easily solved by using the controller output in the adaptation rule instead of the actuator output. For fast motor dynamics (i.e., high cut-off frequency and low DC-gain), we can safely assume that utilizing the controller and the actuator outputs leads to a similar adaptation behavior. Moreover, based

on our unreported simulations, using the controller output leads to a faster convergence in the presence of actuator saturation. This can be explained by the fact that the controller output, compared to the saturated-actuator output, is a better approximation for the desired force for the perfect tracking. Therefore, it is not only practical, but also beneficial to use the controller output for the adaptation.

## VIII. CONCLUSIONS

Due to nonlinear dynamics (i.e., nonlinearity of applied torques w.r.t. joint angles), adaptation of nonlinear compliances has more flexibility to reduce the energy consumption, compared to a linear mechanism. In this paper, we presented such adaptation mechanism for nonlinear variable parallel compliance in order to improve energy efficiency of robotic systems in cyclic tasks. The theoretical aspects of the proposed method were studied rigorously in terms of stability, convergence, and optimality. We presented the notion of residual force; i.e., part of the controller force which cannot be compensated by parallel compliance. We also observed that the residual force creates unsatisfactory, but tolerable, conditions such as rippling in the adaptation. We showed that the adaptation method is a force-squared-minimizer. The relation between force-square minimization and average power minimization was also investigated in theory, simulation, and experiment. In addition, it was shown for PD controllers that the adaptation also reduces the tracking error. This cooperative behavior between controller and adaptive compliance to reduce the tracking error improves the closed-loop performance.

The simulations on simple and complex robotic systems showed that our method works satisfactorily and has the potential to decrease energy consumption more than the linear methods; e.g., simulations on the mass-spring and the manipulator systems. Also in the discussion section, we studied the effects of undesirable conditions (e.g., damping effect and lack of force sensor) on the adaptation rule and presented some alternative approaches to overcome them. Experimental results of the 1-DOF revolute joint supported our theories in practice where satisfactory results were achieved despite of all considerable deviations from our theoretical assumptions and

presence of uncertainties. Furthermore, based on the presented experiment, we can strongly claim that adapting the nonlinear compliances with multi basis functions not only in theory and simulations but also in the real world can improve the energy efficiency in comparison with the linear adaptive compliance. Moreover, these experimental results showed that adaptive compliant structures can enable weak actuators/motors to track cyclic motions; i.e., this results in having lighter and energy efficient robots. Benefiting from the current technology of variable compliance actuators, our method can be easily implemented in robotic systems in order to improve their energy efficiency in cyclic tasks.

## APPENDIX

### A. Linear independent basis functions

The Wronskian determinant can be used to check if the basis functions at  $j$ th joint are the linearly independent; see [39, pp. 500]. The basis function of  $j$ th joint are linearly independent under the following necessary conditions.

A1 : The followings are non-zero and bounded.

$$\left\{ q, \frac{dq}{dt}, \dots, \frac{d^{m-1}q}{dt^{m-1}} \right\}$$

A2 : The followings are continuous w.r.t.  $q$ .

$$\left\{ \phi_i, \frac{\partial \phi_i}{\partial q}, \frac{\partial^2 \phi_i}{\partial q^2}, \dots, \frac{\partial^{m-1} \phi_i}{\partial q^{m-1}} \right\} \quad \text{for } i = 1, \dots, m$$

Having these conditions satisfied along with non-identically-zero Wronskian determinant, the basis functions of  $j$ th joint are linearly independent.

### B. Desired force decomposition

To prove [Theorem.1](#), first, we show the presented decomposition is the solution of the following minimization problem.

$$\tilde{K} = \arg \min_K \underbrace{\int_T F_{res}^2 dt}_{J} \stackrel{(Eq. 6)}{=} \arg \min_K \underbrace{\int_T (F_d + K^T \Phi_d)^2 dt}_{J}$$

To show this, first, we extend the cost function:

$$J = \int_T F_d^2 dt + 2K^T \int_T F_d \Phi_d dt + K^T \underbrace{\int_T \Phi_d \Phi_d^T dt}_{\Omega^{-1}(Eq. 7)} K$$

Partial derivative w.r.t.  $K$  leads to the solution of this minimization problem ( $\tilde{K}$ ) which is presented in [Eq. 7](#).

$$\left. \frac{\partial J}{\partial K} \right|_{K=\tilde{K}} = 0 \Rightarrow 2 \int_T F_d \Phi_d dt + 2\Omega^{-1} \tilde{K} = 0 \quad (14)$$

Finally, the value of this cost function after the minimization yields the residual force ( $F_{res}$ ) as stated in [Eq. 6](#). Moreover, to prove [Eq. 8](#), we multiply [Eq. 6](#) by  $\Phi_d^T$  and integrate it over  $T$ .

$$\underbrace{\int_T F_d \Phi_d^T dt}_{-\tilde{K}^T \Omega^{-1}(Eq. 7)} = -\tilde{K}^T \underbrace{\int_T \Phi_d \Phi_d^T dt}_{\Omega^{-1}(Eq. 7)} + \int_T F_{res} \Phi_d^T dt \quad (15)$$

After canceling  $-\tilde{K}^T \Omega^{-1}$  from both sides, it yields [Eq. 8](#).

### C. Offline compliance optimization

[Eq. 7](#) can be used for offline compliance optimization where  $F_d$  can be pre-computed by knowing the dynamics ([Eq. 4](#)). In case of unknown dynamics, applied force ( $F_a$ ) can be recorded by running the system once, and solving the following equation.

$$K_{opt} = -\left( \int_T \Phi \Phi^T dt \right)^{-1} \int_T F_a \Phi dt$$

In this equation,  $\Phi$  is the vector of basis functions which is a function of joint position and  $F_a$  is applied force by controller which satisfies [Assumption 1](#). To tune the compliance in an offline fashion, this equation just needs the compliance basis functions, position of the joint, and the applied force over a period of time.

### D. Adaptation dynamics

By putting [Eq. 1](#), [Eq. 5](#), and [Eq. 6](#) together, the applied force ( $F_a$ ) can be expressed as<sup>9</sup>:

$$\begin{aligned} F_c &= \Phi^T K \\ F_a &= F_d + F_c + F_e \Rightarrow F_a = \Phi^T K - \Phi_d^T \tilde{K} + F_{res} + F_e \\ F_d &= -\Phi_d^T \tilde{K} + F_{res} \end{aligned} \quad (16)$$

Substituting [Eq. 16](#) in [Eq. 2](#) yields [Eq. 9](#).

### E. Stability analysis and convergence proof

1) *Theorem 2.1*: In [Eq. 9](#),  $\epsilon$  and  $\tilde{K}$  are fixed and the rest of parameters are either function of  $q$  or  $q_d$  and their derivatives. As  $q$  and  $q_d$  are functions of time, we can rewrite [Eq. 9](#) as

$$\dot{K} = -\epsilon \Phi \Phi^T K + f(t); \quad f(t) = \epsilon \Phi (\Phi_d^T \tilde{K} - F_{res} - F_e) \quad (17)$$

where according to [Assumption 1](#),  $f(t)$  is bounded. In this case,  $f(t)$  can be seen as an external disturbance for the following dynamical system.

$$\dot{K}_s = -\epsilon \Phi \Phi^T K_s \quad (18)$$

To investigate stability of this system, we employ the "Barbalat's Lemma" (see [43, pp. 323]). Consider the positive definite Lyapunov function as  $V = 0.5 K_s^T K_s$ . Computing the time derivative of the presented Lyapunov function results in

$$\dot{V} = K_s^T \dot{K}_s = -\epsilon K_s^T \Phi \Phi^T K_s = -\epsilon (K_s^T \Phi)^2$$

where  $\dot{V}$  is negative semidefinite. Therefore, according to Lyapunov stability theorem,  $K_s$  is bounded. The second time derivative of the presented Lyapunov function is

$$\ddot{V} = -2\epsilon K_s^T (\Phi \Phi^T)^2 K_s - 2\epsilon K_s^T \dot{\Phi} \Phi^T K_s$$

As mentioned before,  $K_s$ ,  $q$  and its derivatives are bounded and due to proper selection of the basis functions (sufficiently smooth and linearly independent bases),  $\dot{V}$  is bounded. This implies  $\dot{V}$  is uniformly continuous in time.

We have satisfied all the conditions of Barbalat lemma. Therefore,  $\dot{V} \rightarrow 0$  as  $t \rightarrow \infty$ . Hence,  $K_s^T \Phi \rightarrow 0$  as  $t \rightarrow \infty$ . It is concluded that  $K_s = 0$ , as the only equilibrium point of [Eq. 18](#), is globally asymptotically stable equilibrium. Finally, in [Eq. 17](#), due to bounded property of  $f(t)$ , it could not disrupt the bounded property of  $K$ .

<sup>9</sup>Note that  $F_c$  is scalar and  $K^T \Phi = \Phi^T K$ .

2) *Theorem 2.2*: For periodic  $q$ ,  $\Phi$  and error ( $e$ ) are periodic functions of time. Hence, based on [Assumption 1](#),  $F_e$  is also periodic. Therefore, the conditions for applying the "Averaging Theorem" (see [43, pp. 404]) are satisfied. In this case, the average solution ( $K_{avg}$ ) of [Eq. 9](#) over each cycle, can be extracted as follows.

$$\dot{K}_{avg} = -\epsilon(\Lambda K_{avg} - \Gamma \tilde{K} - K_e) ; \Lambda = \int_T \Phi \Phi^T dt \quad (19)$$

$$K_e = - \int_T \Phi (F_{res} + F_e) dt \quad ; \quad \Gamma = \int_T \Phi \Phi_d^T dt \quad (20)$$

The dynamical equation in [Eq. 19](#), can be written as follows.

$$\dot{K}_{avg} = -\epsilon \Lambda (K_{avg} - (\Lambda^{-1}(\Gamma \tilde{K} + K_e))) \quad (21)$$

In [Eq. 21](#),  $(\Lambda^{-1}(\Gamma \tilde{K} + K_e))$  can be seen as the equilibrium point of this system which minimizes  $F_a^2$  on a period of time. Also  $\Lambda$  is a positive definite matrix which makes  $-\epsilon \Lambda$  a negative definite matrix. Therefore,  $K_{avg}$  exponentially converges to  $(\Lambda^{-1}(\Gamma \tilde{K} + K_e))$ . As the result, [Eq. 9](#) is, on average, exponentially stable.

3) *Theorem 2.3*: In case of perfect tracking ( $q_d \equiv q$ ),  $F_e \equiv 0$  and  $\Phi_d \equiv \Phi$ . Therefore [Eq. 9](#) is simplified as follows.

$$\dot{K} = -\epsilon(\Phi_d \Phi_d^T \Delta K + \Phi_d F_{res}) \quad ; \quad \Delta K = K - \tilde{K} \quad (22)$$

Using "Averaging Theory", [Eq. 22](#) yields to:

$$\dot{K}_{avg} = -\epsilon \Omega^{-1} \Delta K_{avg} \quad ; \quad \Delta K_{avg} = K_{avg} - \tilde{K} \quad (23)$$

which is obtained by omitting  $\Phi_d F_{res}$  (based on [Eq. 8](#)) and replacing  $\Phi_d \Phi_d^T$  by  $\Omega^{-1}$  (based on [Eq. 7](#)). For the truncated dynamics ([Eq. 23](#)),  $\Delta K_{avg} = 0$  is an equilibrium point and  $\Omega^{-1}$  is a positive-definite matrix which makes  $-\epsilon \Omega^{-1}$  a negative-definite matrix. Therefore, equilibrium point of [Eq. 23](#) is globally exponentially stable which implies that  $K$ , on average, exponentially converges to  $\tilde{K}$ . Moreover, based on [Eq. 16](#), applied force ( $F_a$ ) on average converges to the residual force ( $F_{res}$ ). It can also be inferred from [Eq. 22](#) and [Appendix-E1](#) that CCM case ( $F_{res} \equiv 0$ ) results in exact convergence.

#### F. Control effort minimization

1) *Theorem 3.1*: Without imposing any assumption on the controller structure or tracking performance, the applied force at the joint level can be calculated as

$$F_a = h(\ddot{q}, \dot{q}, \bar{q}) + F_w + K^T \Phi(q) \quad ; \quad h : \mathbb{R}^{n \times n \times n} \rightarrow \mathbb{R} \quad (24)$$

where  $h$  represents dynamics of the joint under consideration,  $F_w \in \mathbb{R}$  is external disturbance, and  $K^T \Phi(q) \in \mathbb{R}$  is compliance applied force. Using the gradient of the cost function ([Eq. 10](#)) and [Eq. 24](#) for updating yields  $\dot{K} = -\lambda \nabla_K J(t) = -2\lambda F_a(t) \Phi$ . Choosing  $\epsilon = 2\lambda$ , implies the proposed adaptation rule ([Eq. 2](#)). Note that in this theorem, we did not impose any constraint on the tracking. Thus, force-square-minimization property of our method is always present.

2) *Theorem 3.2*: The solution to the cost function in [Eq. 11](#) is  $\Lambda^{-1}(\Gamma \tilde{K} + K_e)$ . This can be shown by following the same procedure in [Appendix-B](#) and using [Eq. 5](#), [Eq. 6](#), and [Eq. 20](#). In [Theorem 2](#), we showed that compliance, on average, converges to this point. Therefore, we can infer that, the adaptation law, on average, minimizes the cost function in [Eq. 11](#).

#### G. Motion tracking enhancement

1) *Corollary 1.1*: According to [Theorem 3](#), the compliance adaptation results in  $F_a^2$  minimization. Thus, having  $F_a = k_p e + k_d \dot{e}$  for the PD controller, we can conclude that compliance adaptation results in instantaneous  $(k_p e + k_d \dot{e})^2$  minimization.

2) *Corollary 1.2*: Using PD controller force in [Eq. 12](#), we have the following expanded cost function.

$$J_T = \int_{t-T}^t (k_p^2 e^2 + k_d^2 \dot{e}^2) du + 2k_p k_d \int_{t-T}^t e \dot{e} du$$

For periodic motions, the second term is identically zero as shown below.

$$\int_{t-T}^t e \dot{e} du = 0.5(e^2(t) - e^2(t-T)) = 0$$

Therefore, based on [Theorem 3](#), for periodic motions, compliance adaptation results in minimization of [Eq. 12](#).

#### H. Mechanical energy consumption minimization

The desired trajectory ( $q_d$ ) is a pre-defined signal and at a given time, it is fixed. The assumption of perfect tracking ( $q \equiv q_d$ ) implies the same situation for the real trajectory ( $q$ ). Therefore, in the perfect tracking case,  $q$  along with  $\dot{q}$  are pre-defined. Thus, instantaneous optimization of  $|F_a \dot{q}_r|$  and  $|F_a|$  are equivalent. Moreover, optimization of  $|F_a|$  and  $F_a^2$  are equivalent; same gradient direction. Therefore, the proposed adaptation method, in perfect tracking case, minimizes the instantaneous mechanical energy consumption.

#### I. Normalized adaptation rule

1) *Optimality*: Consider the dynamical equation of the joint presented in [Eq. 24](#). In order to extract the normalized adaptation rule, we apply the Newton gradient method on the cost function ( $J = F_a^2$ ) as

$$\dot{K} = -\epsilon(\nabla_K^2 J)^{-1} \nabla_K J \quad , \quad \nabla_K J = 2\Phi F_a \quad , \quad \nabla_K^2 J = 2\Phi \Phi^T$$

Replacing  $\Phi \Phi^T$  with its average over one cycle which is invertible ([Theorem 1](#)) results in [Eq. 13](#). According to these mathematics, the original ([Eq. 2](#)) and the normalized ([Eq. 13](#)) adaptation rules optimize the same cost function ( $J = F_a^2$ ).

2) *Stability and convergence*: By following the same procedure as in [Appendix-D](#), the dynamics of normalized adaptation rule ([Eq. 13](#)) can be extracted as  $\Omega$  multiplied by [Eq. 9](#).

$$\dot{K} = -\epsilon \Omega (\Phi \Phi^T K - \Phi \Phi_d^T \tilde{K} + \Phi (F_{res} + F_e))$$

Since  $\Omega$  is a positive definite matrix and [Eq. 9](#) is convergent and stable, the normalized adaptation rule ([Eq. 13](#)) is also convergent and stable to the equilibrium point of [Eq. 9](#).

3) *Uncoupled dynamics*: With the assumption of perfect tracking, adaptation dynamics for the normalized rule ([Eq. 13](#)) can be obtained similar to [Eq. 23](#) as  $\dot{K}_{avg} = -\epsilon(K_{avg} - \tilde{K})$ . As it can be seen, the adaptation of each element in  $K_{avg}$  is uncoupled from the rest (absence of  $\Omega$  as in [Eq. 23](#)) which results in independent convergence behaviors. Also based on the simple exponential behavior of this 1st order dynamical equation, the 2%-settling-time is  $t_s = 4/\epsilon$ . This settling time

is calculated under ideal assumptions (i.e., perfect tracking and averaging theory) and differs in practice; see Section V. However, in similar cases (e.g., linear vs. nonlinear case in Fig. 3a and Tab. I), the same adaptation rate ( $\epsilon$ ) results in a similar convergence behavior.

### J. Computation of total energy consumption

The mechanical energy consumption of the actuation system responsible for the compliance adaptation is computed as  $E_c = \sum_{k=1}^m \int_0^t |\dot{q}_{ac}^k F_{ac}^k| dt + E_{loss}$  where there are  $m$  motors (for  $m$  basis functions) changing the compliance profile with  $F_{ac}^k$  as the applied force and  $\dot{q}_{ac}^k$  as the velocity of the  $k$ th motor's shaft.  $E_{loss}$  refers to energy loss due to friction, electrical and mechanical imperfections, and so on. To develop this equation, one requires a model for the adaptive compliance that can relate these two variables under a given state of the system. However, to reach a theoretical lower-bound for  $E_c$  in general cases (i.e., when such model for the compliance is not available), we can utilize the total energy of the compliance; i.e., sum of kinetic and potential energies<sup>10</sup>.

$$E = K^T Z + 0.5M\dot{q}^2; \quad Z = [z_1 \ z_2 \dots z_m]^T, \quad Z = \int_0^q \Phi(y) dy$$

Taking the time derivative of the above equation results in  $\dot{E} = \dot{K}^T Z + K^T \Phi \dot{q} + M\dot{q}\dot{q}$  where the first term is caused by compliance adaptation, the second term is the transferred power between the system and the compliance, and the third term is the inertia effect; that is negligible due to small value of  $M$ . Thus, the energy consumption for compliance adaptation ( $E_c$ ) is the integral of the first term. Here, we consider the worst scenario, where the negative work cannot be recycled and there is no energy exchange between the basis functions. Therefore, we have  $E_c = \sum_{i=1}^m \int_0^t |\dot{k}_i z_i(q)| dt$ . Finally, the lower bound of total energy consumption is

$$E_t = \int_0^t |\dot{q} F_a| dt + \sum_{i=1}^m \int_0^t |\dot{k}_i z_i(q)| dt$$

where the first term is the consumed mechanical energy. Multiplying this lower bound with a constant larger than one and adding a constant value to that gives an approximation of the real energy consumption. The values of these constants depend on the adaptation mechanism.

### K. Damped adaptation rule

Consider  $J_m = F_a^2 + \alpha K^T K$  as the modified cost function which penalizes high values of  $K$ . Applying the gradient operator (as in Appendix-F) results in the damped adaptation rule presented in Section VII-C, where  $\epsilon = 2\lambda$  and  $\beta = 2\lambda\alpha$ . By adding the  $-\beta K$  term to the procedure in Appendix-E3, we can see the stable equilibrium for  $K$  (in Eq. 23) is moved from  $\tilde{K}$  to:

$$\tilde{K}_m = \Omega_m \int_T F_d \Phi_d dt; \quad \Omega_m = \left( \frac{\beta}{\epsilon} I + \int_T \Phi_d \Phi_d^T dt \right)^{-1}$$

It is clear that in this case, the existence of  $\Omega_m$  (i.e., the matrix inversion) is guaranteed for  $\beta \neq 0$ .

<sup>10</sup> $M$  is the inertia of the compliant element.

### ACKNOWLEDGMENT

We would like to thank University of Tehran for providing support for this work. Authors would also like to thank Hamed Jalali, Omid Mohseni, and Amir Sarabi for their comments on the first draft of this paper.

### REFERENCES

- [1] G. Tonietti, R. Schiavi, and A. Bicchi, "Design and control of a variable stiffness actuator for safe and fast physical human/robot interaction," in *Proceedings of the 2005 IEEE International Conference on Robotics and Automation*. IEEE, 2005, pp. 526–531.
- [2] T. D. Niehues, P. Rao, and A. D. Deshpande, "Compliance in parallel to actuators for improving stability of robotic hands during grasping and manipulation," *The International Journal of Robotics Research*, p. 0278364914558016, 2015.
- [3] A. Jafari, N. G. Tsagarakis, and D. G. Caldwell, "A novel intrinsically energy efficient actuator with adjustable stiffness (awas)," *IEEE/ASME Transactions on Mechatronics*, vol. 18, no. 1, pp. 355–365, 2013.
- [4] N. Schmit and M. Okada, "Optimal design of nonlinear springs in robot mechanism: simultaneous design of trajectory and spring force profiles," *Advanced Robotics*, vol. 27, no. 1, pp. 33–46, 2013.
- [5] A. Jafari, N. G. Tsagarakis, and D. G. Caldwell, "Awas-ii: A new actuator with adjustable stiffness based on the novel principle of adaptable pivot point and variable lever ratio," in *Robotics and Automation (ICRA), 2011 IEEE International Conference on*. IEEE, 2011, pp. 4638–4643.
- [6] W. Roosting, Z. Li, G. Medrano-Cerda, D. Caldwell, and N. Tsagarakis, "Development and control of a compliant asymmetric antagonistic actuator for energy efficient mobility," *Mechatronics, IEEE/ASME Transactions on*, vol. 21, no. 2, pp. 1080–1091, 2016.
- [7] R. Furnemont, G. Mathijssen, T. van der Hoeven, B. Brackx, D. Lefeber, and B. Vanderborght, "Torsion macepa: A novel compact compliant actuator designed around the drive axis," in *Robotics and Automation (ICRA), 2015 IEEE International Conference on*. IEEE, 2015, pp. 232–237.
- [8] B. Vanderborght, A. Albu-Schäffer, A. Bicchi, E. Burdet, D. G. Caldwell, R. Carloni, M. Catalano, O. Eiberger, W. Friedl, G. Ganesh *et al.*, "Variable impedance actuators: A review," *Robotics and Autonomous Systems*, vol. 61, no. 12, pp. 1601–1614, 2013.
- [9] G. Mathijssen, D. Lefeber, and B. Vanderborght, "Variable recruitment of parallel elastic elements: Series-parallel elastic actuators (spea) with dephased mutilated gears," *Mechatronics, IEEE/ASME Transactions on*, vol. 20, no. 2, pp. 594–602, 2015.
- [10] M. Grimmer, M. Eslamy, S. Glicch, and A. Seyfarth, "A comparison of parallel-and series elastic elements in an actuator for mimicking human ankle joint in walking and running," in *Robotics and Automation (ICRA), 2012 IEEE International Conference on*. IEEE, 2012, pp. 2463–2470.
- [11] T. Verstraten, P. Beckerle, R. Furnemont, G. Mathijssen, B. Vanderborght, and D. Lefeber, "Series and parallel elastic actuation: Impact of natural dynamics on power and energy consumption," *Mechanism and Machine Theory*, vol. 102, pp. 232–246, 2016.
- [12] M. Uemura, G. Hidemasa, and K. Sadao, "Motion control with stiffness adaptation for torque minimization in multijoint robots," *Robotics, IEEE Transactions on*, vol. 30, pp. 352–364, 2014.
- [13] R. M. Alexander, *Principles of animal locomotion*. Princeton University Press, 2003.
- [14] —, "Three uses for springs in legged locomotion," *Robotics Research*, vol. 9, no. 2, pp. 53–61, 1990.
- [15] S. Rutishauser, A. Sprowitz, L. Righetti, and A. J. Ijspeert, "Passive compliant quadruped robot using central pattern generators for locomotion control," in *IEEE RAS & EMBS International Conference on Biomedical Robotics and Biomechatronics, 2008.*, 2008, pp. 710–715.
- [16] Y. Fukuoka, H. Kimura, and A. H. Cohen, "Adaptive dynamic walking of a quadruped robot on irregular terrain based on biological concepts," *Robotics Research*, vol. 22, no. 3-4, pp. 187–202, 2003.
- [17] K. C. Galloway, J. E. Clark, and D. E. Koditschek, "Variable stiffness legs for robust, efficient, and stable dynamic running," *Journal of Mechanisms and Robotics*, vol. 5, no. 1, p. 011009, 2013.
- [18] M. Khoramshahi, A. Sprowitz, A. Tuleu, M. N. Ahmadabadi, and A. Ijspeert, "Benefits of an active spine supported bounding locomotion with a small compliant quadruped robot," in *International Conference on Robotics and Automation*, 2013, pp. 173 229–173 229.

- [19] D. P. Ferris, M. Louie, and C. T. Farley, "Running in the real world: adjusting leg stiffness for different surfaces," *Proceedings of the Royal Society of London. Series B: Biological Sciences*, vol. 265, no. 1400, pp. 989–994, 1998.
- [20] Z. Shen and J. Seipel, "Animals prefer leg stiffness values that may reduce the energetic cost of locomotion," *Journal of theoretical biology*, vol. 364, pp. 433–438, 2015.
- [21] T. McGeer, "Passive dynamic walking," *the international journal of robotics research*, vol. 9, no. 2, pp. 62–82, 1990.
- [22] S. Collins, A. Ruina, R. Tedrake, and M. Wisse, "Efficient bipedal robots based on passive-dynamic walkers," *Science*, vol. 307, no. 5712, pp. 1082–1085, 2005.
- [23] R. Tedrake, T. W. Zhang, and H. S. Seung, "Learning to walk in 20 minutes," in *Proceedings of the Fourteenth Yale Workshop on Adaptive and Learning Systems*, 2005.
- [24] M. Khoramshahi, R. Nasiri, A. Ijspeert, and M. N. Ahmadabadi, "Energy efficient locomotion with adaptive natural oscillator," in *Dynamic Walking 2014*, 2014.
- [25] R. Nasiri, M. Khoramshahi, and M. N. Ahmadabadi, "Design of a nonlinear adaptive natural oscillator: Towards natural dynamics exploitation in cyclic tasks," in *Intelligent Robots and Systems (IROS), 2016 IEEE/RSJ International Conference on*. IEEE, 2016.
- [26] M. Scheint, M. Sobotka, and M. Buss, "Compliance in gait synthesis: Effects on energy and gait," in *8th IEEE-RAS International Conference on Humanoid Robots*. IEEE, 2008, pp. 259–264.
- [27] —, "Optimized parallel joint springs in dynamic motion: Comparison of simulation and experiment," in *Biomedical Robotics and Biomechanics (BioRob), 2010 3rd IEEE RAS and EMBS International Conference on*. IEEE, 2010, pp. 485–490.
- [28] M. Plooij and M. Wisse, "A novel spring mechanism to reduce energy consumption of robotic arms," in *2012 IEEE/RSJ International Conference on Intelligent Robots and Systems*. IEEE, 2012, pp. 2901–2908.
- [29] A. Mazumdar, S. Spencer, J. Salton, C. Hobart, J. Love, K. Dullea, M. Kuehl, T. Blada, M. Quigley, J. Smith *et al.*, "Using parallel stiffness to achieve improved locomotive efficiency with the sandia steppr robot," in *2015 IEEE International Conference on Robotics and Automation (ICRA)*. IEEE, 2015, pp. 835–841.
- [30] Y. Huang, B. Vanderborght, R. Van Ham, and Q. Wang, "Torque–stiffness-controlled dynamic walking with central pattern generators," *Biological cybernetics*, pp. 1–21, 2014.
- [31] J. Borràs and A. M. Dollar, "Actuation torque reduction in parallel robots using joint compliance," *Journal of Mechanisms and Robotics*, vol. 6, no. 2, p. 021006, 2014.
- [32] V. Duindam and S. Stramigioli, "Optimization of mass and stiffness distribution for efficient bipedal walking," in *Proceedings of IEEE/RSJ International Conference on Intelligent Robots and Systems, Edmonton, Canada*. Citeseer, 2005.
- [33] M. Khoramshahi, A. Parsa, and M. Ijspeert, Auke Nili Ahmadabadi, "Natural dynamics modification for energy efficiency, a data driven parallel compliance design method," in *International Conference on Robotics and Automation (ICRA), 2014*, 2014.
- [34] B. Vanderborght, *Dynamic stabilisation of the biped Lucy powered by actuators with controllable stiffness*. Springer, 2010, vol. 63.
- [35] A. Enoch, A. Sutas, S. Nakaoka, and S. Vijayakumar, "BLUE: a bipedal robot with variable stiffness and damping," in *Humanoid Robots, 2012 IEEE/RAS International Conference on*, 2012.
- [36] D. Braun, M. Howard, and S. Vijayakumar, "Optimal variable stiffness control: formulation and application to explosive movement tasks," *Autonomous Robots*, vol. 33, no. 3, pp. 237–253, 2012.
- [37] R. Ozawa and H. Kobayashi, "A new impedance control concept for elastic joint robots," in *Robotics and Automation, 2003. Proceedings. ICRA'03. IEEE International Conference on*, vol. 3. IEEE, 2003, pp. 3126–3131.
- [38] M. Uemura, S. Kawamura, H. Hirai, and F. Miyazaki, "Iterative motion learning with stiffness adaptation for multi-joint robots," in *International Conference on Robotics and Biomimetics*, 2014, pp. 1088–1093.
- [39] I. N. Bronshtein, K. A. Semendiyayev, G. Musiol, and H. Muehlig, *Handbook of mathematics*. Springer, 2007, vol. 3.
- [40] MATLAB, "Mathworks Inc." 2011. [Online]. Available: <http://www.mathworks.com>
- [41] M. Khoramshahi, H. J. Bidgoly, S. Shafiee, A. Asaei, A. J. Ijspeert, and M. N. Ahmadabadi, "Piecewise linear spine for speed–energy efficiency trade-off in quadruped robots," *Robotics and Autonomous Systems*, vol. 61, no. 12, pp. 1350–1359, 2013.
- [42] S. Mozaffari, E. Rekabi, R. Nasiri, and M. N. Ahmadabadi, "Design & modeling of a novel multi-functional elastic actuator (mfea)," in *Robotics*

and *Mechatronics (ICROM), 2016 4th RSI International Conference on*. IEEE, 2016.

- [43] H. K. Khalil, *Nonlinear systems*. Prentice hall Upper Saddle River, 2002.



**Rezvan Nasiri** was born in December 1989. He received his B.S. degree in Electrical Engineering from University of Gilan in September 2012. He received M.Sc. in Control Engineering from University of Tehran under Prof. Nili and Prof. Yazdanpanah's supervision in September 2014. He is currently a Ph.D. candidate in Cognitive Robotic Laboratory at University of Tehran. His main research interests are bio-inspired design, legged locomotion, system dynamics, machine learning, and rehabilitation.



**Mahdi Khoramshahi** received his B.Sc. degree in the Electrical Engineering from Sharif University of Technology (2004–2009). He received his M.Sc. in Electrical Engineering from University of Tehran (2009–2012). He carried out as an intern in Biorobotics Laboratory (BioRob) at EPFL under Prof. Auke Ijspeert supervision (2011–2012). He then became a research scholar at NanoRobotics laboratory (Prof. Metin Sitti) at Carnegie Mellon University (2012–2013), and research assistance in Cognitive Robotic Laboratory (Prof. Majid Nili) at

University of Tehran. He is currently a PhD student at Learning Algorithm and System Laboratory (Prof. Aude Billard) at EPFL. His research interests includes cognitive robotics, Human-robot interaction, dynamical systems and control, and machine learning.



**Mohammad Shushtari** was born in December 1990. He received his B.S. degree from IKIU in September 2013. He is currently a graduate student in Cognitive Robotic Laboratory at University of Tehran under Prof. Nili and Prof. Yazdanpanah's supervision. As his thesis project, he is dealing with meta-optimization on energy consumption in robotic systems. His research interests are legged locomotion, nonlinear control, rehabilitation, and dynamical systems.



**Majid Nili Ahmadabadi (M.N. Ahmadabadi)** was born in 1967 and received his B.S from Sharif University of Technology of Iran in 1990. He received his M.Sc. and Ph.D. in Information Sciences from the Graduate School of Information Science, Tohoku University, Japan in 1994 and 1997 respectively. In 1997, he joined the Advanced Robotics Laboratory at Tohoku University. Later he moved to School of Electrical and Computer Engineering, College of Engineering, University of Tehran where he is a professor and the head of Robotics and AI Laboratory. Dr Ahmadabadi is the founder and the director of Cognitive Systems Laboratory as well. He is also a senior researcher at School of Cognitive Sciences, Institute for Research in Fundamental Sciences (IPM), Iran.

He was one of the distinguished lecturers selected by IEEE Robotics and Automation Society for the years 2007–2009. Dr Ahmadabadi served as a member of the engineering board of Iranian National Science Foundation for the period 2005–2011. He is one of the founders of The Robotics Society of Iran in addition to the Iranian Society of Cognitive Sciences. His main research interests are cognitive robotics and modeling cognitive systems in addition to control of legged robots.